논문 99-8-5-3

결합형 유한요소-경계요소 기법을 사용한 심해저용 압전형 유연성 쏘나 트랜스듀서의 구조 설계

장순석, 정운관*

Structural design of a piezoelectric flextentional deep-water sonar transducer using a coupled FE-BEM

Soon Suck Jarng and Woon Kwan Chung*

요 약

결합형 유한요소-경계요소 기법을 사용하여 심해저용 유연형 압전체 쏘나 트랜스듀서를 설계하였다. 쏘나 트랜스듀서의 역학적 구동을 3차원적으로 모델링하였고 전기적 외부 부하 조건을 가지고 분석하였다. 쏘나 트랜스듀서의 정상 상태 변위 모드, 지향성, 공진 주파수, TVR과 같은 결과들을 보였다. 본 논문의 술통 형태의 압전체 쏘나 트랜스듀서를 설계하면서, 심해저용으로 사용하기 위해 쏘나 트랜스듀서의 내외부에 동일한 수압이 가해지도록 쏘나 트랜스듀서의 외부 표면 구조를 새롭게 변형시킨 결과 낮은 주파수의 새로운 공진 모드가 발생하였으나 그 크기는 외부 표면 구조 변형의 정도에 따라 조절될 수 있다.

Abstract

A piezoelectric flextentional deep-water sonar transducer has been designed using a coupled FE-BEM. The dynamics of the sonar transducer is modelled in three dimensions and is analyzed with external electrical excitation conditions. Different results are available such as steady-state frequency response for TX displacement modes, directivity patterns, resonance frequencies, TVRs. While the conventional barrel-stave typed sonar transducer of the piezoelectric material is designed, the external surface of the transducer is modified in order to allow the same hydrostatic pressure to be applied onto the inner and the outer surfaces of the transducer. With this modification for deep-water application, a new resonance mode is generated at lower frequency. This lower resonance mode can be adjusted according to the degree of the outer surface modification.

1. Introduction

Ocean acoustic tomography requires wide bandwidth, compact, and effectively low frequency sources of sound[1]. This paper describes the modelling process for such a sonar transducer using a coupled finite element-boundary element method (FE-BEM). Flextentional sonar transducers are widely used as a high-power projector. It is a compact sound source efficiently over quite a broad frequency range[2]. The precise dimensions of a flextentional sonar transducer could be optimally predicted by the analysis of

조선대학교 전기·제어계측공학부 (Dept. of Electrical Control & Instrumentation, Chosun University)

* 조선대학교 원자력공학과 (Dept. of Nuclear Eng., Chosun University)

<접수일자 : 1999년 7월 21일>

the flextentional transducer dynamics. The choice of the active element depends on structural types and electromechanical efficiency of the transducer. A flextentional transducer such as a barrel-stave type has been modelled in three dimensions. The main aim of this paper is to design the optimal structure of the flooded piezoelectric flextentional sonar transducer using a coupled FE-BEM. Different results for analyses are produced; displacement modes, directivity patterns, resonance frequencies, and transmitting voltage responses. A new design skim is suggested in section 2.5 where the outer surface structure of the other previous barrel-stave type sonar transducer is modified in order to compensate deep-water pressure.

For low-frequency (between 2~5 kHz) and high-power applications flextentional transducers are generally used (Figure 1). Here a stack of ceramic ring, as it expands and contracts as a result of the applied alternating voltage, exerts an oscillatory force on a pair of thick metal "barrel staves" [3]. A bolt holds the staves together and pre-stresses the ceramic stack so that even under high drive the ceramic and any bonds between components remain in compression. With this construction the relatively small linear motion of the ceramic stack is converted into a much larger change in the volume of the staves, so that moderate power levels are possible.

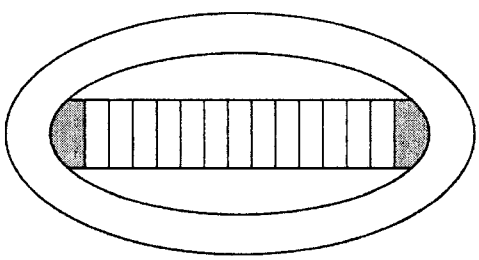

Figure 1. Flextentional sonar transducer prototype for frequency between 2~5 kHz

2. Numerical Method

2.1 Finite Element Method (FEM)

The following equation (1) is the integral formulation of the piezoelectric equations:

$$\begin{aligned} \{F\}+\{F_I\} &= [K_{uu}]\{a\} + [K_{u\phi}]\{\phi\} \\ &\quad -\omega^2[M]\{a\} + j\omega[R]\{a\} \\ -\{Q\} &= [K_{\phi u}]\{a\} + [K_{\phi\phi}]\{\phi\} \end{aligned} \tag{1}$$

where

$\{F\}$	Applied Mechanical Force
$\{F_I\}$	Fluid Interaction Force
$\{Q\}$	Applied Electrical Charge
$\{a\}$	Elastic Displacement
$\{\phi\}$	Electric Potential
ω	Angular Frequency
$[M]$	Mass Matrix
$[R]$	Dissipation Matrix
$[K_{uu}]$	Elastic Stiffness Matrix
$[K_{\phi\phi}]$	Permittivity Matrix
$[K_{u\phi}]$	Piezoelectric Stiffness Matrix
	$[K_{\phi u}]=[K_{u\phi}]^t$

The isoparametric formulation for 3-dimensional structural elements is well documented by Allik H. et. al.[4]. Each 3-dimensional finite element is composed of 20 quadratic nodes and each node has nodal displacement (a_x, a_y, a_z) and electric potential (ϕ) variables. In local coordinates the finite element has 6 surface planes (±xy, ±yz, ± zx) which may be exposed to external fluid environment. The exposed surface is used as a boundary element which is composed of 8 quadratic nodes.

2.2 Boundary Element Method (BEM)

For sinusoidal steady-state problems, the Helmholtz equation, $\nabla^2\Psi + k^2\Psi = 0$, represents the fluid mechanics. Ψ is the acoustic pressure

with time variation, $e^{j\omega t}$, and $k(=\omega/c)$ is the wave number. In order to solve the Helmholtz equation in an infinite fluid media, a solution to the equation must not only satisfy structural surface boundary condition (BC), $\frac{\partial \Psi}{\partial n} = \rho_f \omega^2 a_n$, but also the radiation condition at infinity, $\lim_{r\to\infty} \oint_S (\frac{\partial \Psi}{\partial r} + jk\Psi)^2 dS = 0$. $\frac{\partial}{\partial n}$ represents differentiation along the outward normal to the boundary. ρ_f and a_n are the fluid density and the normal displacement on the structural surface. The Helmholtz integral equations derived from Green's second theorem provides such a solution for radiating pressure waves;

$$\oint_S \left(\Psi(q) \frac{\partial G_k(p,q)}{\partial n_q} - G_k(p,q) \frac{\partial \Psi(q)}{\partial n_q} \right) dS_q = \beta(p)\ \Psi(p) - \Psi_{inc}(p) \quad (2)$$

where $G_k(p,q) = \frac{e^{-jkr}}{4\pi r}$, $r = |p-q|$

p is any point in either the interior or the exterior and q is the surface point of integration. β(p) is the exterior solid angle at p.

The acoustic pressure for the i^{th} global node, $\Psi(p_i)$, is expressed in discrete form[5]:

$$(\ 1 \le i \le ng\ )$$

$$\beta(p_i)\ \Psi(p_i) - \Psi_{inc}(p_i) = \oint_S \left(\Psi(q) \frac{\partial G_k(p_i,q)}{\partial n_q} - G_k(p_i,q) \frac{\partial \Psi(q)}{\partial n_q} \right) dS_q \quad (3a)$$

$$= \sum_{m=1}^{nt} \int_{S_m} \left(\Psi(q) \frac{\partial G(p_i,q)}{\partial n_q} - G(p_i,q) \frac{\partial \Psi(q)}{\partial n_q} \right) dS_q \quad q \in S_m \quad (3b)$$

$$= \sum_{m=1}^{nt} \int_{S_m} \left(\sum_{j=1}^{8} N_j(q)\ \Psi_{m,j} \frac{\partial G(p_i,q)}{\partial n_q} - G(p_i,q) \sum_{j=1}^{8} N_j(q) \frac{\partial \Psi_{m,j}}{\partial n_q} \right) dS_q \quad (3c)$$

$$= \sum_{m=1}^{nt} \sum_{j=1}^{8} \left(\int_{S_m} N_j(q) \frac{\partial G(p_i,q)}{\partial n_q} dS_q \right) \Psi_{m,j} - \rho_f \omega^2 \sum_{m=1}^{nt} \sum_{j=1}^{8} \left(\int_{S_m} N_j(q) G(p_i,q) n_q dS_q \right) a_{m,j} \quad (3d)$$

$$= \sum_{m=1}^{nt} \sum_{j=1}^{8} A^i_{m,j} \Psi_{m,j} - \rho_f \omega^2 \sum_{m=1}^{nt} \sum_{j=1}^{8} B^i_{m,j} a_{m,j} \quad (3e)$$

where nt is the total number of surface elements and $a_{m,j}$ are three dimensional displacements. Equation (3b) is derived from equation (3a) by discretizing integral surface. And equation (3c) is derived from equation (3b) since an acoustic pressure on an integral surface is interpolated from adjacent 8 quadratic nodal acoustic pressures corresponding the integral surface. Then equation (3d) is derived from equation (3c) by swapping integral notations with summing notations. Finally the parentheses of equation (3d) is expressed by upper capital notations for simplicity.

When equation (3e) is globally assembled, the discrete Helmholtz equation can be represented as

$$([A] - \beta[I])\{\Psi\} = +\rho_f \omega^2 [B]\{a\} - \{\Psi_{inc}\} \quad (4)$$

where [A] and [B] are square matrices of (ng by ng) size. ng is the total number of surface nodes.

Where the impedance matrices of equation (4), [A] and [B], are computed, two types of singularity arise[6]. One is that the Green's function of the equation, $G_k(p_i,q)$, becomes infinite as q approaches to p_i. This problem is solved by mapping such rectangular local coordinates into triangular local coordinates and again into polar local coordinates[7]. The other is that at certain wave number the matrices become ill-conditioned. These wave number are corresponding to eigenvalues of the interior Dirichlet problem[8]. One approach to overcome the matrix singularity is that [A] and [B] of equation (4) are modified to provide a unique solution for

the entire frequency range[9~12]. The modified matrix equation referred to as the modified Helmholtz gradient formulation (HGF)[12] is obtained by adding a multiple of an extra integral equation to equation (4).

$$([A]-\beta[I]\oplus\alpha[C])\{\Psi\} = +\rho_f\,\omega^2([B]\oplus\alpha[D])\{a\}-(\Psi_{inc}\oplus\alpha\frac{\partial\Psi_{inc}}{\partial n_p}) \tag{5}$$

where

$$\alpha=-\frac{1}{k\cdot(\textit{Number of surface elements adjacent a surface node})}$$

[C] and [D] are rectangular matrices of (nt by ng) size. nt is the total number of surface elements. $\oplus$ symbol indicates that the rows of [C],[D] corresponding to surface elements adjacent a surface node are added to the row of [A],[B] corresponding to the surface node, that is,

$$\sum_{i=1}^{ng}\sum_{j=1}^{ng}A(i,j)=\sum_{i=1}^{ng}\sum_{j=1}^{ng}A(i,j)+\sum_{i=1}^{ng}\sum_{j=1}^{ng}\Big(\sum_{m=1}^{S(i)}\alpha\,C(m,j)\Big)$$
$$\sum_{i=1}^{ng}\sum_{j=1}^{ng}B(i,j)=\sum_{i=1}^{ng}\sum_{j=1}^{ng}B(i,j)+\sum_{i=1}^{ng}\sum_{j=1}^{ng}\Big(\sum_{m=1}^{S(i)}\alpha\,D(m,j)\Big) \tag{6}$$

where S(i) is the number of surface element adjacent a surface node. The derivation of the extra matrices [C],[D] are well described by Francis[12]. Equation (6) may be reduced in its formulation using superscript $\oplus$ for convenience;

$$A^{\oplus}\{\Psi\} = +\rho_f\,\omega^2B^{\oplus}\{a\} - \Psi^{\oplus}_{inc} \tag{7}$$

where

$$([A]-\beta[I]\oplus\alpha[C]) \equiv A^{\oplus}$$
$$([B]\oplus\alpha[D]) \equiv B^{\oplus}$$
$$(\Psi_{inc}\oplus\alpha\frac{\partial\Psi_{inc}}{\partial n_p}) \equiv \Psi^{\oplus}_{inc}$$

Equation (7) can be written as

$$\{\Psi\} = +\rho_f\,\omega^2(A^{\oplus})^{-1}B^{\oplus}\{a\}-(A^{\oplus})^{-1}\Psi^{\oplus}_{inc} \tag{8}$$

2.3 Coupled FE-BE Method

The acoustic fluid loading on the solid-fluid interface generates interaction forces. These forces can be related to the surface pressures by a coupling matrix [L][5,13];

$$\{F_f\} = -[L]\{\Psi\} \tag{9}$$

where $[L] = \int N^t n N dS$. N is a matrix of surface shape functions and n is an outward normal vector at the surface element. N^t is the transposed form of N matrixes.

Equations (8) and (9) indicate that the interaction force can be expressed by functions of elastic displacement instead of acoustic pressure. This relationship can be applied to equation (1) when the sonar transducer model is submerged into the infinite fluid media:

$$\{F\}+[L](A^{\oplus})^{-1}\Psi^{\oplus}_{inc} = [K_{uu}]\{a\}+[\rho_f\,\omega^2[L](A^{\oplus})^{-1}B^{\oplus}]\{a\} + [K_{u\phi}]\{\phi\}-\omega^2[M]\{a\}+j\omega[R]\{a\}$$
$$-\{Q\} = [K_{\phi u}]\{a\}+[K_{\phi\phi}]\{\phi\} \tag{10}$$

where

$\Psi^{\oplus}_{inc}$	Incident Pressure
$[L]$	Coupling Matrix at the Fluid-Structure Interface
$A^{\oplus}$	Fluid BEM Matrix [A]
$B^{\oplus}$	Fluid BEM Matrix [B]
ρ_f	Fluid Density
$j=\sqrt{-1}$	

Since the present sonar transducer is modelled as a projector, the internal force vector, $\{F\}$, and the external incident pressure, $[L](A^{\oplus})^{-1}\Psi^{\oplus}_{inc}$, of equation (10) are removed. The only applied BC for the equation is the applied electrical charge vector, $\{Q\}$. The acoustic pressure in the far field is determined by $\beta(p)=1$ for given values of surface nodal pressure and surface nodal displacement;

$$\Psi(p_i) = \sum_{m=1}^{nt}\sum_{j=1}^{8}A^i_{m,j}\Psi_{m,j} - \rho_f\,\omega^2\sum_{m=1}^{nt}\sum_{j=1}^{8}B^i_{m,j}a_{m,j}-(A^{\oplus})^{-1}\Psi^{\oplus}_{inc} \tag{11}$$

2.4 Modelling of a barrel-stave typed piezoelectric sonar transducer

Instead of using the piezoelectric ceramic itself in a flexural mode, it is possible to devise flextentional structures in which the high stress but low strain generation of the ceramic in the thickness mode is transformed into larger displacements by means of some type of level action (Figure 1 ~ Figure 3). A stack of piezoelectric ceramic operating in the thickness mode is connected to a surrounding elliptical shell like a barrel-stave. When the stack extends, along the major axis of the ellipse, the shell moves inwards along the minor axis, thus producing a large volume displacement overall. In general terms, the resonance frequency of such a transducer depends principally on the major and minor axes, wall thickness, and material properties of the shell, with the stack itself having a lesser influence[11]. The bandwidth is also dependent primarily on the parameters of the shell. Maximum eccentricity leads to the maximum bandwidth, but has the lowest power output, whilst least bandwidth and highest power occurs for the least eccentric shape[14]. The maximum pressure which an elliptical shell can withstand is also dependent on its shape and thickness, and is therefore related to its resonance frequency. The size of the flextentional transducer is generally much less than a wavelength in water at their resonance frequency. It therefore radiates approximately omni- directionally in the plane perpendicular to the major axis. A compressive pre-stress needs to be applied to the stack for higher power output from a compact size. This is usually done by applying pressure to the minor axis of the shell, thus extending the major axis, and inserting the stack into the extended shell. On release of the pressure, the relaxation of the shell applies the necessary force to the stack.

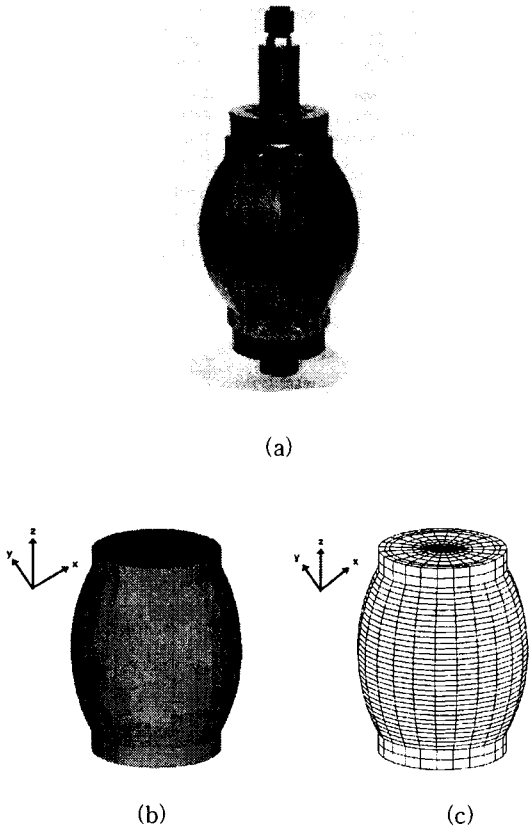

Figure 2. External view of the flextentional sonar transducer (a) and their corresponding finite mesh elements in 3 dimensions (b) and (c).

The piezoelectric flextentional sonar transducer has been totally divided into 608 elements with 3280 nodes. The solid-fluid interfacing surface elements are 320 with 992 nodes. Only one fourth of the total elements are used for formulation of the global coefficient matrix because of the symmetricity of the structure as shown in Figure 3 (b). Figure 4 shows the dimensions of the one eighth of the barrel-stave transducer in meter scale. The dimensions of the modelled transducer are not optimal, however the dimensions could be changed for any particular optimal purpose.

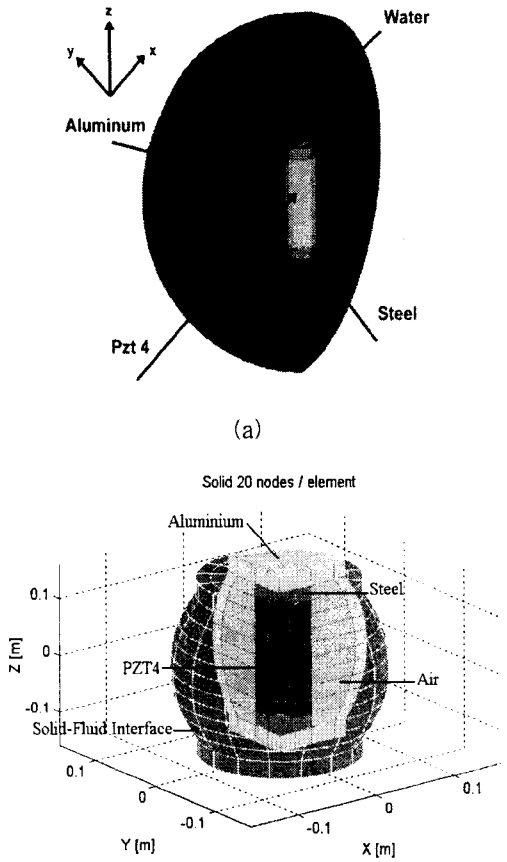

Figure 3. Three dimensional view of the flextentional sonar transducer within the fluid domain (a) and the internal materialistic composure of the modelled sonar transducer (b).

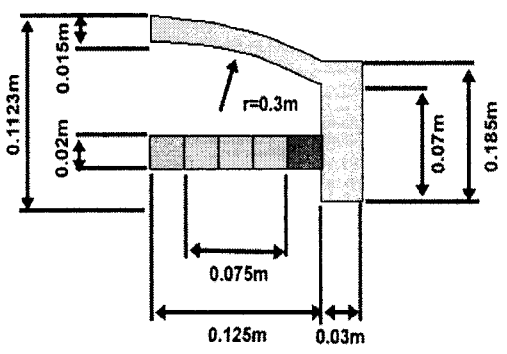

Figure 4. The dimensions of the 1/8 of the flextentional sonar transducer. r=curvature radius.

Table 1 and Table 2 show property values of the materials used for the sonar transducer.

Table1. Piezoelectric Material Properties of PZT4 (Axially Polarized Properties)

Parameter	Value	Unit	Parameter	Value	Unit
ρ	7500	kg/m^3	C_{xy}^{xy}	3.06E+10	N/m^2
C_x^x	1.39E+11	N/m^2	$e_{p,z}^x$	-5.2	N/Vm
C_y^x	7.78E+10	N/m^2	$e_{p,z}^y$	-5.2	N/Vm
C_z^x	7.43E+10	N/m^2	$e_{p,z}^z$	15.1	N/Vm
C_y^y	1.39E+11	N/m^2	$e_{p,z}^{yz}$	12.7	N/Vm
C_z^y	7.43E+10	N/m^2	$e_{p,z}^{zx}$	12.7	N/Vm
C_z^z	1.15E+11	N/m^2	ε_x^x	6.46E-9	F/m
C_{yz}^{yz}	2.56E+10	N/m^2	ε_y^y	6.46E-9	F/m
C_{zx}^{zx}	2.56E+10	N/m^2	ε_z^z	5.62E-9	F/m
K_{33}	0.69	-	K_{15}	0.70	-

Table 2 Properties of other materials used for the flextentional sonar transducer

Property / Material	Density ρ [kg/m^3]	Young's Modulus Y [N/m^2]	Poison's Ratio γ
Air	1.22	1.411E5	-
Aluminium	2750	70.0E9	0.34
Steel	7850	207.0E9	029

2.5 Modelling of a barrel-stave typed sonar transducer with pressure compensation gaps

So far, the inside of the present flextentional sonar transducer is only filled with air (or water). If the air-filled flextentional sonar transducer is submerged into deep water, the external surface of the barrel-stave is pushed into the inside by high hydrostatic pressure. This deep-water pressure problem causes weakening of the structural displacements, so that the output acoustic power becomes low. This problem can be solved by allowing the sea water to be penetrated into the inside of the transducer by some slight modification of the external surface of the

barrel-staves typed flextentional transducer as shown in Figure 5. Very narrow and long openings are made between staves, so that the inner and the outer surfaces of the stave have equal water pressure. Since the piezoelectric elements are directly exposed to water pressure loading, the resonance frequency of the modified flextentional sonar transducer becomes lower than that of the non-modified flextentional sonar transducer because of mass loading effects.

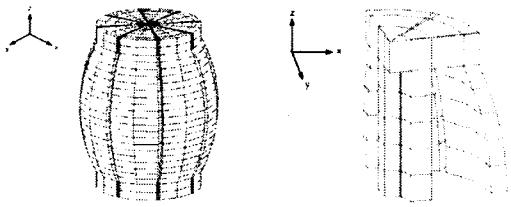

(a) (b)

Figure 5. The barrel-stave typed deep-water sonar transducer with hydrostatic pressure compensation gaps between staves (a) and its 1/8 internal finite element meshes.

3. Results and Discussions

The coupled FE-BE method has been programmed with Fortran language running at a SUN workstation. Calculation is done with double precision and the program is made for three dimensional structures. It is a common practice to have the size of the largest element to be less than $\lambda/3$.

Figure 6 shows the transmitting voltage (TV) responses of the air-filled flextentional submerged transducer. The acoustic power at 4785 Hz resonance is about 147 dB (ref 1 μPa/1V at 1m) at Z axis direction. And figure 7 shows beam patterns in polar form for different input frequencies.

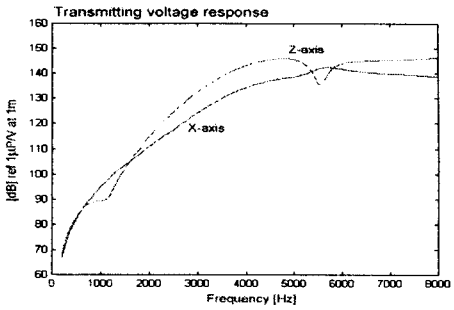

Figure 6. Transmitting voltage response of air-filled flextentional transducer in dB (ref 1 μPa at 1m)(0° :X-axis, 90° :Z-axis).

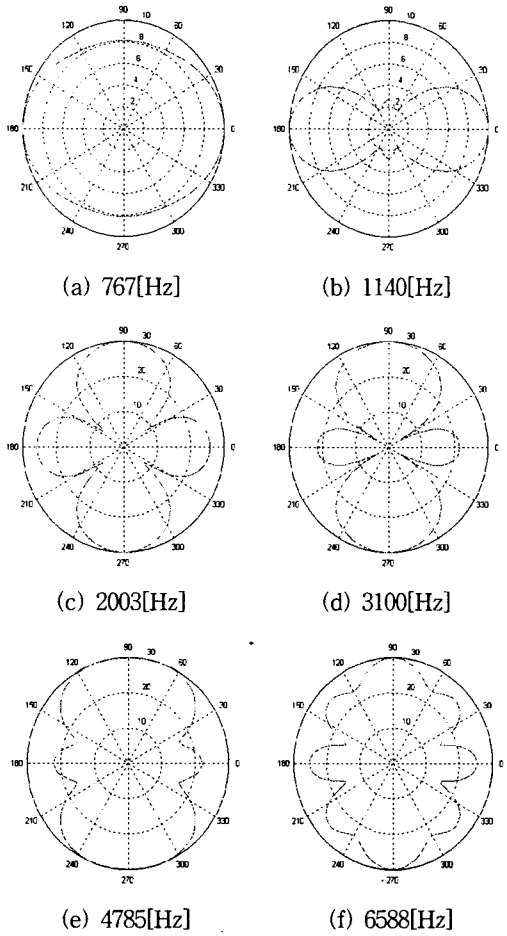

(a) 767[Hz] (b) 1140[Hz]

(c) 2003[Hz] (d) 3100[Hz]

(e) 4785[Hz] (f) 6588[Hz]

Figure 7. Beam patterns for different input frequencies (0° :X-axis, 90° :Z-axis).

Figure 8 shows the transmitting voltage (TV) responses of the water-filled flextentional transducer. The acoustic power at 3766 Hz resonance is about 148 dB (ref 1 μPa/1V at 1m) at Z axis direction. And figure 9 shows beam patterns for different input frequencies. The water-filled flextentional sonar transducer has a lower resonance frequency than the air-filled flextentional sonar transducer, but the output acoustic power seems not to be changed.

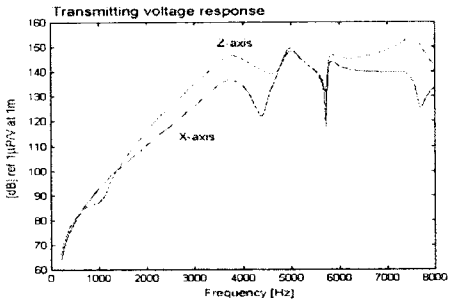

Figure 8. Transmitting voltage response of water-filled flextentional transducer in dB (ref 1 μPa at 1m)(0° :X-axis, 90° :Z-axis).

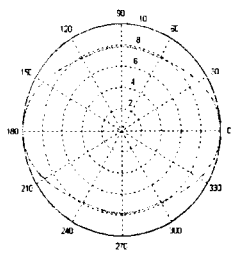

(a) 767[Hz]

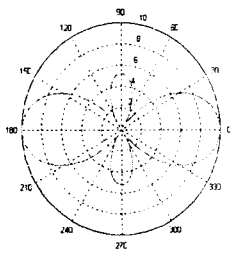

(b) 1140[Hz]

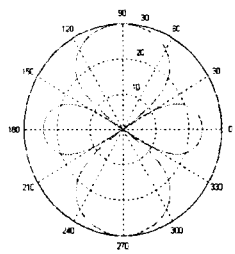

(c) 2003[Hz]

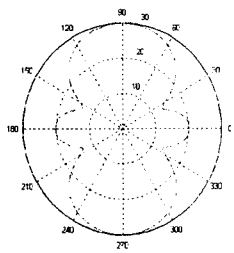

(d) 3766[Hz]

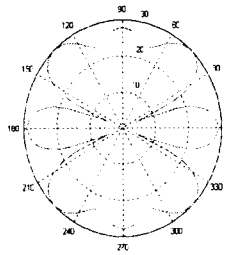

(e) 4981[Hz]

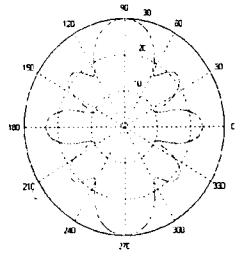

(f) 6588[Hz]

Figure 9. Beam patterns for different input frequencies (0° :X-axis, 90° :Z-axis).

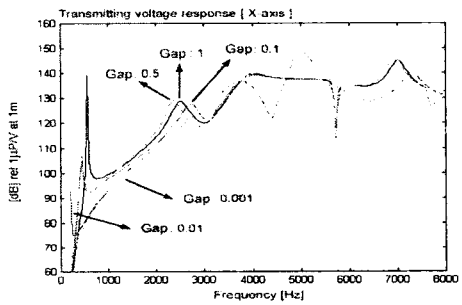

(a)

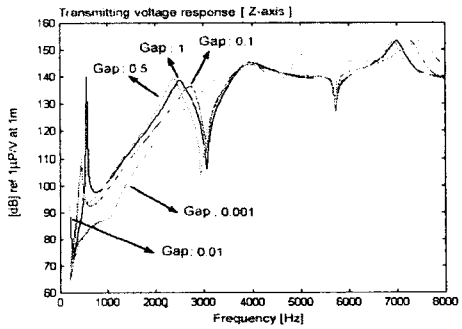

(b)

Figure 10. Transmitting voltage response of pressure-compensated flextentional transducer for different gaps in dB (ref 1 μPa at 1m) (0° :X-axis (a), 90° :Z-axis (b)).

Figure 10 shows the transmitting voltage (TV) responses of the modified pressure-compensated flextentional transducer. The acoustic power at

2~3 kHz resonance is about 135 dB (ref 1 μPa/1V at 1m) at Z axis direction for different opening gaps. The pressure-compensated flextentional sonar transducer has a more lower resonance frequency than the water-filled flextentional sonar transducer, but the output acoustic power seems to be lower than the latter one. The sizes of the opening gaps are noticed in figures.

Figure 11 shows the resonance frequency variation of the pressure-compensated flextentional sonar transducer with different opening gaps. For the present model, the sonar transducer with 0.5° opening gap produces the lowest resonance frequency. And figure 12 shows beam patterns with 0.5° gap for different input frequencies.

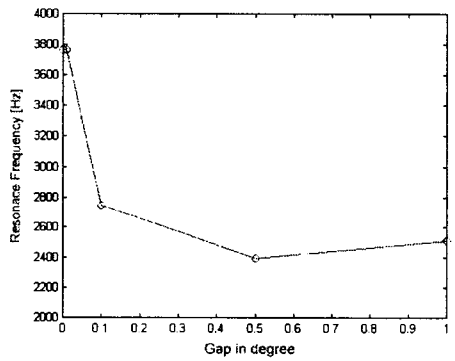

Figure 11. Variation of resonance frequency of the pressure-compensated flextentional sonar transducer with different gaps in degree.

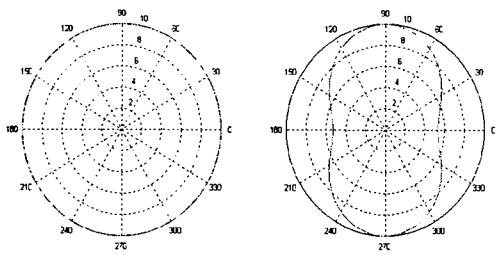

(a) 552[Hz] (b) 1140[Hz]

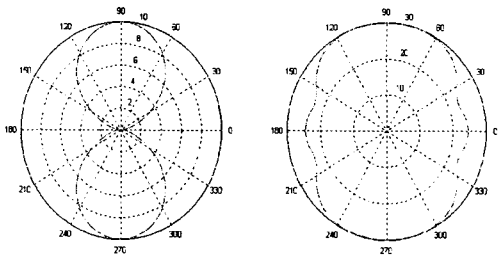

(c) 2521[Hz] (d) 4041[Hz]

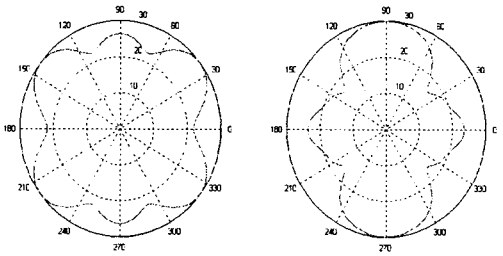

(e) 6001[Hz] (f) 7020[Hz]

Figure 12. Beam patterns of the pressure-compensated flextentional deep-water sonar transducer with 0.5° opening gap , (0° :X-axis, 90° :Z-axis).

Figure 13 shows the displacement modes of the one eighth of the pressure-compensated flextentional transducer at 2521 Hz with 21 different phases. The figures are plotted with hidden lines in series for 1/20 intervals of one cycle, so that the change of the structural displacement can be viewed in different phases. From the series of figures in different phases, it is clear to notice that the force generated by the active element is transferred to the aluminium stave through the end caps in the similar mechanism like an arm lever. Therefore the relatively small linear motion of the ceramic stack is converted into a much larger change in the volume of the staves. Figure 14 shows the same displacement mode as figure 13 at one particular phase but at Z-axis view point.

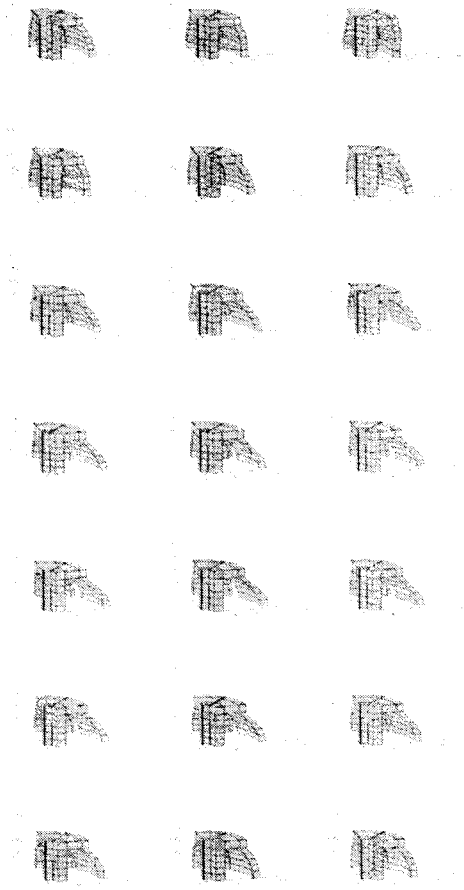

Figure 13. Displacement modes of the one eighth pressure-compensated flextentional transducer at 2521 Hz with 21 different phases.

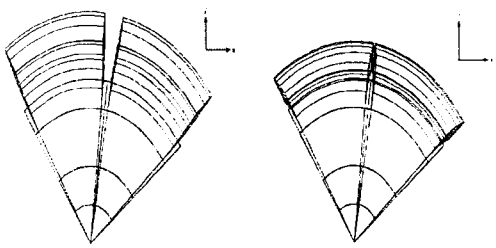

(a) (b)

Figure 14. Displacement modes of the pressure-compensated flextentional transducer at 2512 [HZ] (opening gap: 0.5°), (a): real value, (b): imaginary value. (view point of (a),(b): Z-axis).

4. Conclusion

The dynamics of the barrel-stave sonar transducer of the piezoelectric material had been simulated using a coupled FE-BEM. The flextentional displacement mode was temporally figured to show the mode in different phases. The conventional flextentional sonar transducer is modified in order to compensate the hydrostatic pressure. The pressure-compensated flextentional sonar transducer produces lower resonance frequency as well as lower output acoustic power than the conventional flextentional sonar transducer. This paper does not include the effect of hydrostatic pressure which is significantly important for deep water operation. More advanced structural design should be considered for deep-water application such as a free-flooded flextentional transducer.

ACKNOWLEDGEMENTS

This study was supported by a grant from STEPI (Science and Technology Policy Institute) Korea under contract I-03-020-A-020, as part of the 1998 international programme of collaboration between Korea and the United Kingdom and by a grant from the European Community under contract MAS3-CT95-0031 (BASS).

References

[1] D.T.I. Francis, J. Ahmad, C. Bayliss and R.F.W. Coates, "Finite and bounadry element modelling of class III flextentional transducers for ocean acoustic tomography", Proc. Second European Conf. Underwater Acoustics, Vol. 1, pp:515-520, 1994.

[2] D.T.I. Francis, C. Bayliss, J. Ahmad and R.F.W. Coates, "The development of a low frequency barrel-stave transducer for

tomographic application using finite element and boundary element modelling", IEEE Proc. Oceans 94, Vol. 1, pp:371-376, 1994.

[3] B.V. Smith, "Lecture notes on basic electromechanical transducer equivalent circuits for underwater applications", Edited by B. Gazey, P. McQueen and B. Smith, Post-Experience Cource on Underwater Acoustics and Sonar Systems, Vol. 1, Chapter 6, 1989.

[4] H. Allik and T.J.R. Hughes, "Finite element method for piezoelectric vibration", Int. J. Numer. Method Eng., Vol. 2, PP:151-157, 1970.

[5] L.G. Copley, "Integral equation method for radiation from vibrating bodies", J. Acoust. Soc. Am. Vol. 41, PP:807-816, 1967.

[6] L.G. Copley, "Fundamental results concerning integral representations in acoustic radiation", J. Acoust. Soc. Am. Vol. 44, PP:28-32, 1968.

[7] E. Skudrzyk, "The foundation of acoustics", (Springer-Verlag, New York, 1971), PP:408-409, Equation(76), 1971.

[8] D.T.I. Francis, "A boundary element method for the analysis of the acoustic field in three dimensional fluid-structure interaction problems", Proc. Inst. of Acoust., Vol. 12, Part 4, PP:76-84, 1990.

[9] H.A. Schenck, "Improved integral formulation for acoustic radiation problems", J. Acoust. Soc. Am. Vol. 44, PP:41-58, 1968.

[10] A.J. Burton and G.F. Miller, "The application of integral integration methods to the numerical solutions of some exterior boundary problems", Proc. R. Soc. London, Ser. A 323, PP:201-210, 1971.

[11] R.F. Kleinman and G.F. Roach, "Boundary integral equations for the three dimensional Helmholtz equation", SIAM Rev., Vol. 16, PP:214-236, 1974.

[12] D.T.I. Francis, "A gradient formulation of the Helmholtz integral equation for acoustic radiation and scattering", J. Acoust. Soc. Am. Vol. 93(4) Part 1, PP:1700-1709, 1993.

[13] O.C. Zienkiewicz, D. Kelly and P. Bettess, "The coupling of finite element method and boundary solutions procedures", Int. J. Num. Methods Eng., Vol. 11, PP:355-375, 1977.

[14] J. Ahmad, D.T.I. Francis and R.F.W. Coates, "A fluid-filled flextentional device for ocean acoustic tomography", IEEE Proc. Oceans 95, Vol. 3, pp: 2021-2026, 1995.

著 者 紹 介

장 순 석

『센서학회지 제7권 제6호』 논문98-7-6-01 p.1참조

현재 조선대학교 전기제어계측공학부 부교수

정 운 관

1955년 9월 9일생

1975~1985년 한양대학교 원자력공학과 수학 (공학박사), 1979~1982년 한양대학교 원자력공학과 조교, 1982~1988년 경희대학교 원자력공학과 전임강사, 현재 조선대학교 원자력공학과 교수

주관심분야 : 방사선방어